Available online at www.sciencedirect.com

Manufacturing Letters

Manufacturing Letters 35 (2023) 208–214

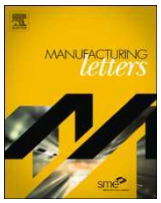

51st SME North American Manufacturing Research Conference (NAMRC 51, 2023)

Analysis of the AISI 316 Stainless Steel Sheet Response to Sub-zero Deformation Temperatures

S. Bruschi[a], E. Simonetto[a], M. Pigato[a], A. Ghiotti[a], R. Bertolini[a]

[a]*Dept. of Industrial Engineering, University of Padova, Via Venezia 1, 35131, Padova, Italy*

* Corresponding author. Tel.: +39 049 8276819; fax: +39 049 8276819. E-mail address: stefania.bruschi@unipd.it

Abstract

Sheet forming carried out at sub-zero temperatures is gaining interest for deforming metal sheets to increase formability while avoiding the need for subsequent heat treatments after forming at elevated temperatures. This paper investigates the feasibility of conducting sub-zero deformation on AISI 316 stainless steel sheets at temperatures ranging from -100°C to 700°C at varying rolling directions. The mechanical and microstructural features were evaluated after deformation as well as the corrosion resistance. The obtained results showed that deformation at -50°C induced a substantial increase of the uniform elongation and slightly higher hardness, but lower corrosion resistance, compared to testing at room temperature and at 300°C and 700°C.

Keywords: AISI 316; cryogenic temperature; uniform elongation; strain-induced martensitic transformation

1. Introduction

Austenitic stainless steels are widely used for a variety of applications in different industrial sectors, such as automotive, biomedical, aerospace, energy, food and nuclear, due to their high corrosion resistance, good ductility, and reasonable cost. However, the major drawback is still their quite low mechanical strength, because face-centered cubic (FCC) austenite is a soft phase. During cold working processes, the strain-induced martensitic transformation (SIMT) may occur, leading to the so-called transformation-induced plasticity (TRIP) effect, which increases the steel work hardening capacity and affects its ductility. Furthermore, the presence of martensite is known to decrease corrosion resistance. The need to decrease SIMT in forming corrosion-resistant parts has driven interest in forming at elevated temperatures below the recrystallization temperature. In warm forming, dynamic recovery takes place, preventing SIMT from occurring, but, at the same time, decreasing work hardening and the final strength of the component.

The forming limits of AISI 304 stainless steel sheets were experimentally investigated [1], indicating the potential for SIMT suppression and formability enhancement at temperatures lower than 150 °C. The influence of the warm forming temperature on the mechanical performances of AISI 304 parts tested under cryogenic environments was evaluated in [2], proving that the warm-formed material exhibited higher cryogenic mechanical properties in terms of ductility and impact toughness than the one formed at room temperature.

Recently, sheet forming processes carried out at sub-zero temperatures have been investigated as an alternative to room temperature and high temperature-assisted forming processes with the twofold objective to: i) enhance the metal sheet formability thanks to the necking onset delay, and ii) avoid possible heat treatments after the forming process in case of high temperature testing. Furthermore, forming at sub-zero temperatures can assure higher work hardening, leading to

enhanced mechanical strength compared to room and elevated temperature forming.

These findings are confirmed by several scientific literature studies; nevertheless, most of them are devoted to aluminum alloy sheets, neglecting stainless steel.

In the study by [3], the discontinuous deformation bands in aluminum-lithium alloys were significantly reduced at cryogenic temperatures. In [4] AA7075 sheet samples were subjected to tensile tests at varying stress triaxiality at temperatures ranging from -100 °C to 300 °C, proving an increase of the ultimate tensile stress (UTS) and deformation at necking when deforming at sub-zero temperatures, regardless of the stress triaxiality. This was ascribed to the formation of a higher amount of precipitates and suppression of dynamic recovery compared to room and high temperature testing. The cryogenic deformation behavior of the same aluminum alloy was investigated in [5], but tempered at different conditions: when cryogenic deformed in W-tempered condition, the alloy exhibited a drastic increase of its ductility, which was attributed to the suppression of the Portevin-Le Chavelier (PLC) effect, activation of additional slip systems as well as enhanced work hardening. The damage and fracture behavior of AA7075 sheets deformed at cryogenic temperatures were modeled in [6] making use of the phenomenological GISSMO fracture model, which was then validated through the cryogenic stamping of a U-shaped part. A lower damage value was predicted in the sidewall of the cryogenic stamped part. In [7] a deep drawing process for deforming Al-Cu-Mn alloy sheets at cryogenic temperatures was proposed, which made it possible to manufacture parts with just slightly localized thinning, uniform thickness distribution, and higher limiting drawing ratio compared to room temperature forming.

To the best of the author's knowledge, besides aluminum alloys, few other metal sheets have been tested at cryogenic temperatures with their behavior contrasted with room and warm forming conditions. The plasticity and fracture characteristics of alpha titanium sheets deformed from -180 °C to 200 °C were analyzed in [8], demonstrating a significant improvement of the necking strain limit at cryogenic temperatures, whereas the fracture strain limit was drastically increased at warm temperatures. The former was ascribed to the synergistic effects of slip and twinning, which increased the dislocation mobility and refined the grain size. The behavior of thin pure copper sheets was investigated in [9], suggesting that the increased strength and ductility at cryogenic temperatures were due to a higher dislocation density and more homogeneous dislocation distribution.

It is worth noting that, except in the case of alpha titanium, the above-reported sheet metals deformed at cryogenic temperatures are all characterized by a FCC structure, suggesting a strong sensitivity of this crystal lattice to microstructural rearrangement at sub-zero temperatures. Nevertheless, a review of the scientific literature highlights a lack of knowledge on the effect of sub-zero deformation temperatures on the mechanical behavior of austenitic stainless steels with a focus on the formability aspects.

The objective of the present study is to evaluate the deformation and post-deformation characteristics of AISI 316 stainless steel sheets when strained in a wide range of temperatures, from -100 °C to 700 °C. The mechanical characteristics at the uniform elongation are determined as well as the related microstructural features. The post-deformation characteristics are evaluated in terms of microstructure, micro-hardness and corrosion resistance to give a comprehensive insight into the effect of sub-zero deformation on austenitic stainless steel compared to room and warm deformation.

2. Material and methods

2.1. Sheet material

The material under investigation was the AISI 316 stainless steel supplied in form of sheets of 1 mm thickness. Its nominal chemical composition in the as-received condition is reported in Table 1.

Table 1. Chemical composition of the AISI 316 sheets (weight %) [10].

Fe	Cr	Ni	Mo	Mn	Si	C
67.69	16.63	10.85	2.42	0.38	1.28	0.018

Fig. 1 shows the optical microscopy image of the as-received sheet along the rolling direction (RD). The material exhibits a conventional austenitic microstructure with a certain amount of uniformly distributed twins.

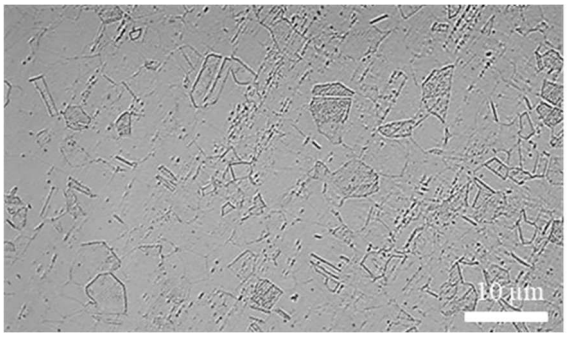

Figure 1. AISI 316 sheet microstructure along the RD in the as-received condition.

2.2 Uniaxial tensile tests

To characterize the uniaxial mechanical behavior of the AISI 316 sheets at different temperatures, dog-bone samples were water-jet cut from the rolled sheets.

Fig. 2 on the right shows the geometry of the samples, having a nominal gauge length l_0 of 65 mm and a nominal gauge w_0 of 12 mm, according to the ISO 6892 standard [11]. The samples were cut both along the sheet rolling direction, hereinafter called *0 deg* samples, and along the orthogonal direction, hereinafter called *90 deg* samples, to assess possible anisotropy effects.

The uniaxial tensile tests were carried out using a hydraulic MTS^{TM} 322 universal test frame with a maximum load capacity of 50 kN. As shown in Fig. 2 on the left, an environmental chamber was used to set the sample testing temperature. Five different temperatures were considered,

for both the *0 deg* and *90 deg* samples, namely -100 °C, -50 °C, 25 °C, 300 °C and 700 °C. To reach testing temperatures below 0 °C, the environmental chamber was connected to a liquid nitrogen (LN_2) tank, from which the LN_2 was collected and its flow was closed loop controlled to reach the target temperature with an accuracy of ± 2 °C. On the contrary, a resistance heating system was used to heat the samples up to 700 °C. The testing temperature of 300 °C and 700 °C were chosen as representative of the warm forming temperature range for the AISI 316 stainless steel. All the tests were performed at a strain rate 0.1 s^{-1}, being within the typical strain rate range of sheet forming operations. Each testing condition was carried out 3 times for sake of repeatability. Two sets of tests were carried out at varying testing temperatures, namely one at fracture to provide the whole stress-strain curve and, thus, identify the UTS for each testing temperature, and the other at UTS to assess the material characteristics at the necking occurrence.

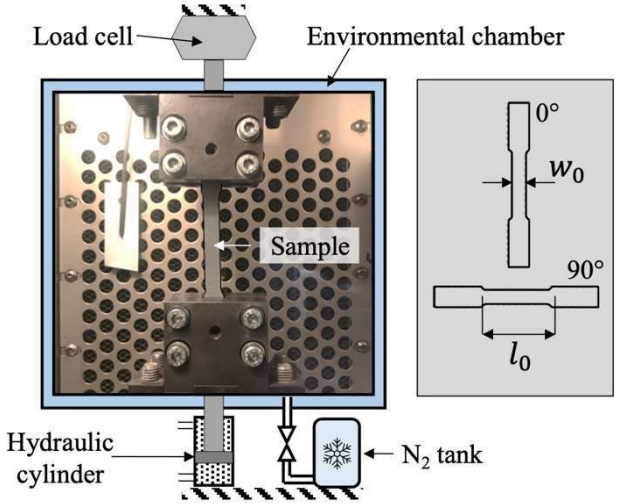

Figure 2. Uni-axial tensile test equipment for sub-zero and elevated temperature testing (geometries of the samples on the right).

2.3 Post-deformation microstructural and mechanical analyses

For investigating the microstructural features induced by mechanical testing, the samples strained at UTS were cut, hot-mounted, and then polished according to the standard metallographic procedures. Then, they were etched by using the Beraha's reagent (1 g $K_2S_2O_5$, 20 ml HCl, and 100 ml H_2O) for 5 s and subsequently inspected by using a Leica DMRE™ optical microscope equipped with a high-definition digital camera. The orientation of the cut samples mounted in the polymer was changed in order to investigate their microstructure with respect to the rolling direction. For each sample, the microstructure was analyzed along the RD, normal (ND), and transverse sections (TD).

The Vickers micro-hardness of the samples strained at UTS was measured using a Leitz Durimet™ micro-hardness tester with a load of 50 gr for 30 s; five values for each section were recorded and then the average value was calculated.

In order to investigate the occurrence of martensite during deformation, X-Ray diffraction (XRD) analyses were performed. After mechanical removal of the surface oxide layer with abrasive papers (500, 800 1200 grit), the samples strained at UTS were electropolished by using the A2 Struers™ electrolyte at 30 V for 60 s. The XRD analyses were carried out using a Siemens™ D500 X-Ray diffractometer, equipped with a monochromator on the detector side and a Cu radiation tube, working at 40 kV and 30 mA. The 2Θ = 40–100 ° angular range was investigated with a step scan of 0.04° and a counting time of 8 s.

2.4 Corrosion resistance analysis

The electrochemical behavior of the samples strained at UTS was evaluated using a standard three electrodes cell, where the strained samples were the working electrode, a Saturated Calomel Electrode (SCE) the reference electrode, and a platinum electrode the counter one.

An Amel™ 2549 potentiostat was used for the electrochemical tests. The potentiodynamic polarization curves were obtained from a starting potential of -1 V below the open circuit potential (OCP) to a potential of 1.2 V, at a scan rate of 0.5 mVs^{-1}. The potentiodynamic polarization curves were obtained through testing in a standard 0.5% saline solution [12].

The corrosion potential (E_{corr}), and the corrosion current density (I_{corr}) were determined from the polarization measurements using the Tafel extrapolation method, according to the ASTM G5-14 standard [12].

3. Results and discussion

3.1. Mechanical response

The results of the tensile tests at varying temperatures ranging from -100 °C to 700 °C are reported in Fig. 3. The engineering stress-strain data, calculated from the load and displacement values recorded by the dynamometer sensors, for the *0 deg* samples are shown in Fig. 3 a), while the data for the *90 deg* samples are reported in Fig. 3 b). The engineering data were chosen and plotted to evaluate both the UTS and strain at necking (e_{neck}) values. The latter identifies when the necking phenomenon occurs: from this point on, the strain localizes in one section, and the sheet thickness sharply decreases till fracture. The uniform elongation, namely e_{neck}, is considered as an indicator of the metal sheet formability.

Regardless of the sample orientation, the UTS increased as temperature decreased while the opposite occurred for increasing the temperature.

Fig. 4 a) shows the UTS percentage variation taking as baseline the data obtained when testing at room temperature. It is worth noticing how UTS increased on average by 24.3 % at -50 °C and by 36.7 % at -100 °C. On the contrary, the UTS average maximum reduction of 47.1 % was obtained at 700 °C compared to room temperature data. Similarly, Fig. 4 b) shows the percentage variation of e_{neck}, taking again as baseline the data obtained at room temperature. For both the *0 deg* and *90 deg* samples, the highest percent increases were obtained at –50 °C, namely 17.8 % for the former and 14.9 % for the latter.

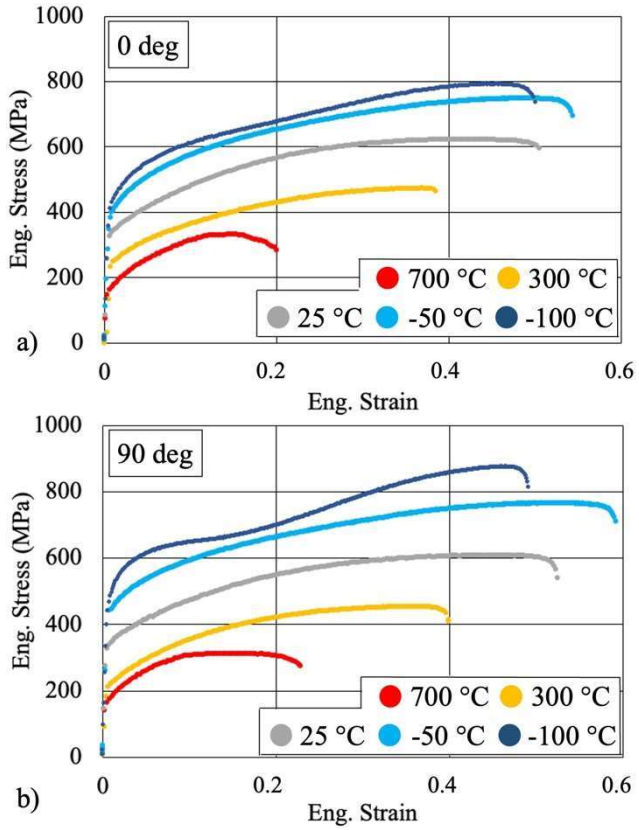

Figure 3. Engineering stress-strain curves at varying temperatures for the a) *0 deg* and b) *90 deg* samples.

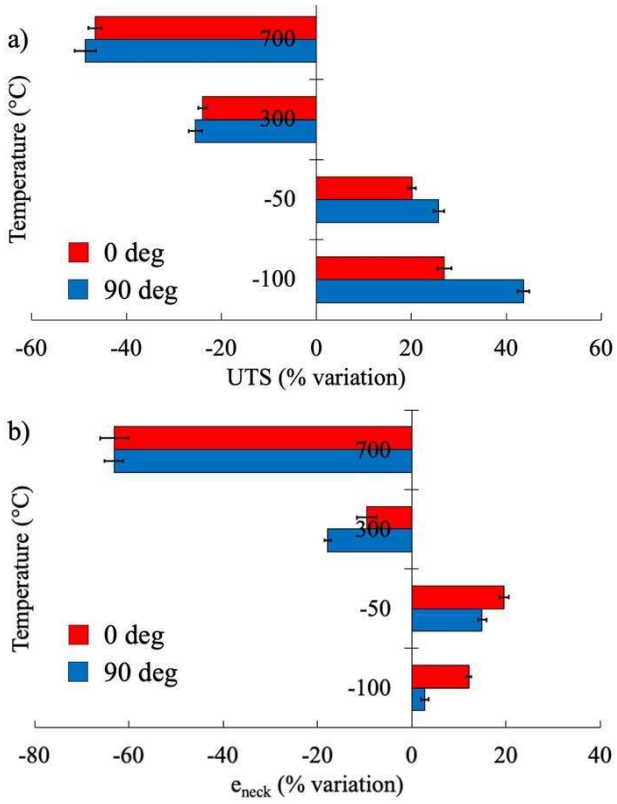

Figure 4. Percentage variation of a) UTS and b) e_{neck}, with respect to the baseline data at room temperature for the *0 deg* and *90 deg* samples.

On the contrary, for the same sample orientations, the increments at -100 °C were limited to 11.0 % and 2.8 %, respectively. On the other hand, the testing temperature increase led to an earlier necking occurrence, with an average percentage reduction of 13.2 % at 300 °C and 60.2 % at 700 °C compared to the room temperature data.

The effect of the testing temperature on the work hardening rate, defined as $d\sigma/de$, was also evaluated and is shown in Fig. 5 a) for the *0 deg* samples and in Fig. 5 b) for the *90 deg* ones. Taking as reference the data obtained at room temperature, in case of forming at sub-zero temperatures, not only the work hardening rate increased but also the plastic instability occurred at higher strain values.

The same Fig. 5 shows also the plastic instability points, which indicate the necking occurrence when the work hardening reaches the zero value, namely necking is delayed when forming below room temperature. The maximum e_{neck} value was reached at -50 °C, while further cooling at -100 °C did not lead to any increase of the uniform elongation.

It is worth noticing how both the work hardening rate and engineering stress-strain curves at -100 °C show an inflection point. These inflection points, highlighted in Fig. 5 and occurring at an engineering strain of 0.16 for the *0 deg* samples and 0.10 for the *90 deg* ones, represent an evident sign of an early transformation of the austenite phase into martensite compared to the one occurring at -50 °C [13]. This early formation of the martensite phase not only affected the curve shape but also reduced the amount of uniform elongation.

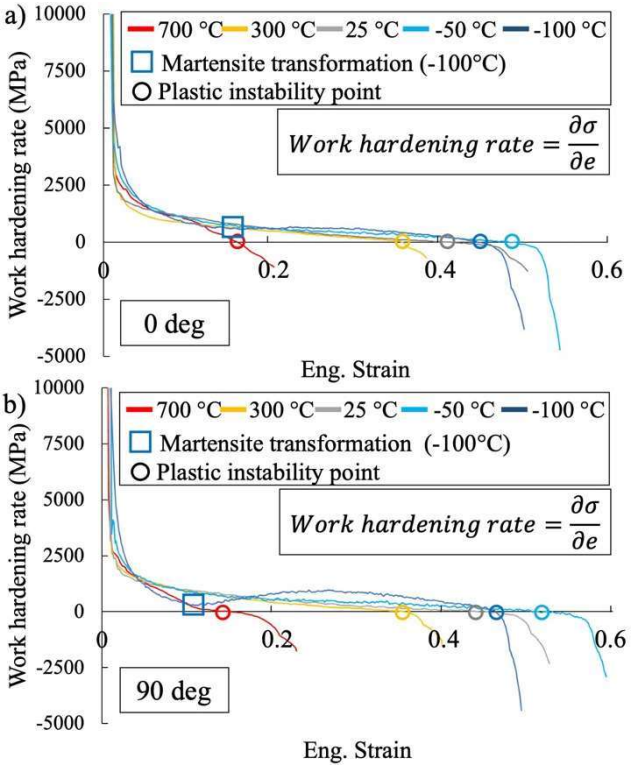

Figure 5. Work hardening rate at varying temperatures for the a) *0 deg* and b) *90 deg* samples.

3.2 Post-deformation microstructural and mechanical characteristics

Fig. 6 shows the microstructure of the *0 deg* samples strained at UTS as a function of the testing temperature and rolling section. It is worth underlining that the post-deformation characterization was focused only on the *0 deg* samples strained at UTS since the effect played by the anisotropy was minor with the respect to the one given by the testing temperature, as commented in § 3.1.

It is evident that testing at temperatures lower than room temperature resulted in martensite formation as a consequence of the higher strains achieved at UTS. The microstructure analysis shows that plate-like α' martensite tended to form as parallel or cross strips in the same austenite grain in the correspondence of the deformation bands [14]. While the martensite phase was barely visible in the sample deformed at 25 °C, its amount was the highest for the sample strained at -100 °C. The microstructures of the samples deformed at 300 °C and 700 °C are not reported since they were not successfully revealed by the etchant used or revealing the martensite phase. In other words, for the samples tested at temperatures higher than room one, the microstructure remained fully austenitic, as a consequence of the occurrence of the dynamic recovery phenomenon that suppressed the SIMT effect.

The XRD results reported in Fig. 7 confirm the presence of martensite in the samples deformed at UTS at sub-zero temperatures. From the width to half height of the martensite diffraction peaks it was possible to quantify the martensite percentage for the *0 deg* samples, which settled at 25 % and 78 % for the samples deformed at UTS at -50 °C and -100 °C, respectively. It is worth noting that the presence of martensite was not detected in the sample tested at 25 °C, being its amount out of the limit of detection of the instrument employed for XRD.

Similarly, for the *90 deg* samples the martensite percentage settle at 35% and 72% for the samples deformed at UTS at -50 °C and -100 °C, respectively being still negligible at 25 °C.

The martensite percentage data are in accordance with the e_{neck} values: at -100 °C the high amount of martensite led to a drastic decrease of ductility, which meant a reduction in the uniform elongation, whereas, at -50 °C, the SIMT effect was not significant enough to affect the steel ductility. Further confirmation of that is given by the M_{d3} temperature, which represents the temperature at which 50 % of martensite is formed at a strain of 0.3 and is indicative of austenite stability. M_{d30} for the present AISI 316 steel settles to -83 °C according to the Nohara calculation, hence it is exceeded only when deforming at -100 °C [15].

Fig. 8 reports the hardness percentage variation taking as baseline the data obtained when testing at room temperature as a function of the testing temperature and rolling section.

The primary role of the deformation temperature in conditioning the material hardness during deformation can be clearly seen in Fig. 8.

In particular, compared to the one at room temperature, the hardness considerably increased only for the material tested at -100 °C, whereas slight improvements were seen for the sample tested at -50 °C. A 22 %, 17 % and 18 % hardness increase was registered for the sample deformed at -100 °C on the ND, RD and TD planes, respectively, with the respect to one of the samples deformed at room temperature.

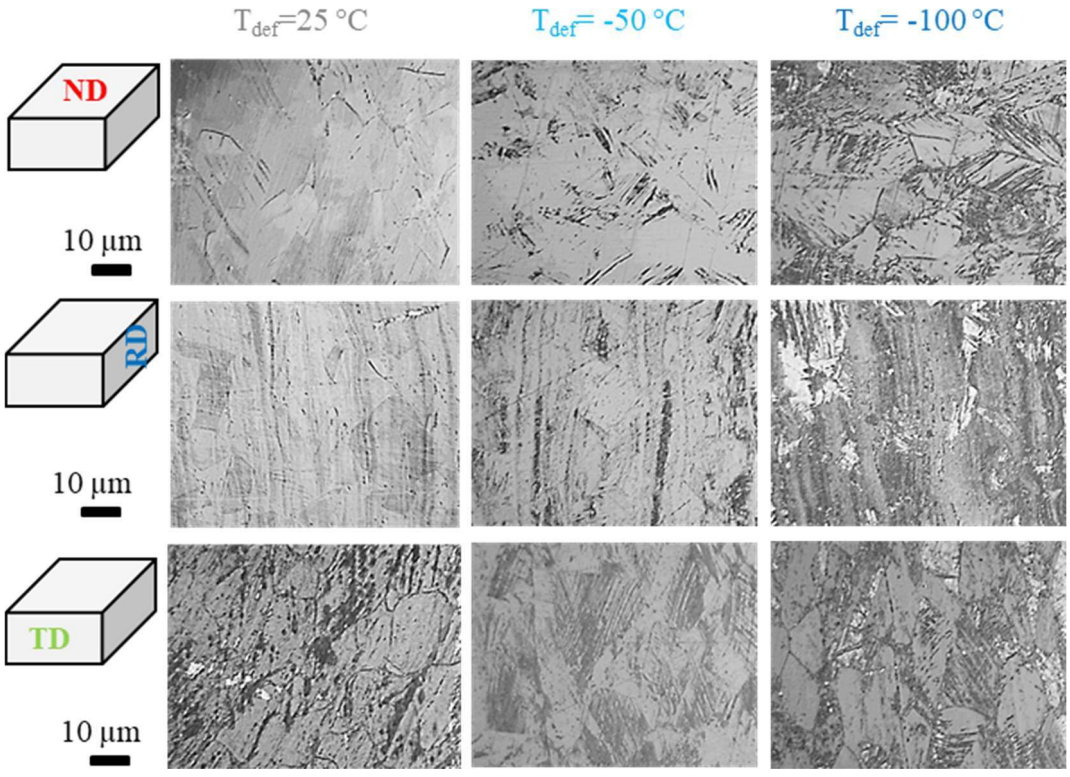

Figure 6. Microstructure of the *0 deg* samples strained at UTS at room and sub-zero testing temperatures.

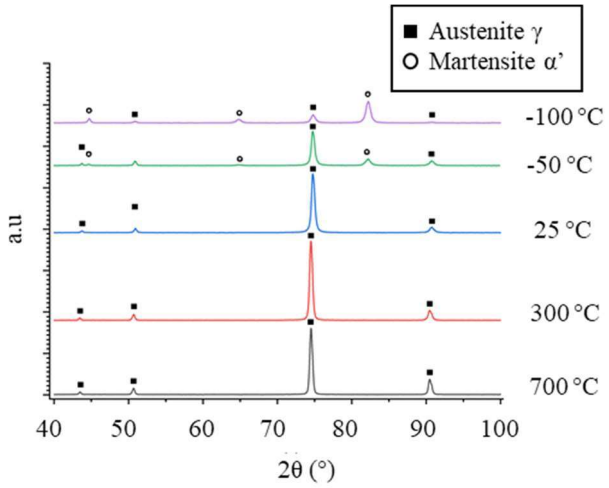

Figure 7. XRD diffraction peaks of the *0 deg* samples strained at UTS.

On the contrary, a drastic decrease in hardness is visible for the samples tested at temperatures higher than the room one. Specifically, the hardness of the sample deformed at 700 °C decreased of 37 %, 27 % and 30 % on the ND, RD and TD planes, respectively, with respect to one of the sample deformed at room temperature. These hardness outcomes are in accordance with the microstructures reported in Fig. 6, which shows the highest amount of martensite content when the material was deformed at -100 °C, and, therefore, the highest hardness.

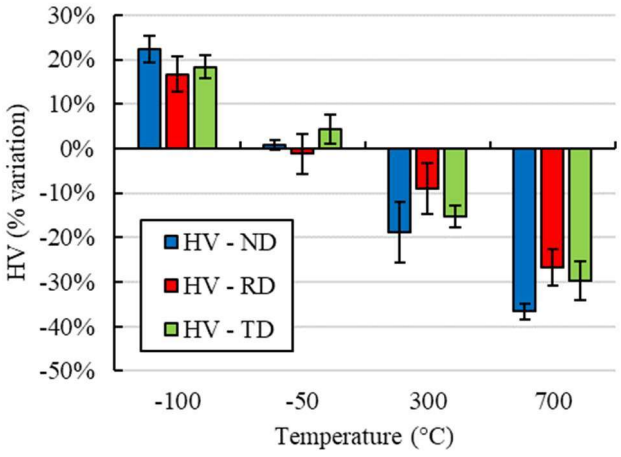

Figure 8. Percentage variation of hardness of the *0 deg* samples strained at UTS with respect to the baseline data obtained at room temperature at varying testing temperature and rolling section.

3.3 Post-deformation corrosion resistance

The potentiodynamic polarization curves of the *0 deg* samples strained at UTS are shown in Fig. 9 as a function of the testing temperature, whereas Table 2 reports the electrochemical parameters extrapolated from the corrosion curves.

The corrosion current, which is directly connected to the corrosion rate through Faraday's law, is very sensitive to the testing temperature. While the samples deformed at UTS at 25 °C, 300 °C and 700 °C show comparable values of the corrosion current, deforming at sub-zero temperatures make it increases significantly. Specifically, a 900 % and a 3400 % increase in I_{corr} was found for the sample tested at -100°C and -50 °C with the respect to the ones deformed at 25 °C, whereas a reduction of 55 % and 50 % was found at 300 °C and 700 °C, respectively.

The corrosion potentials settle to approximately the same value for all the investigated samples, except for the one deformed at -100 °C that showed a E_{corr} decrease in accordance with the previous data.

The aforementioned results can be explained on the basis of: i) the microstructure variation induced by the deformation at sub-zero temperatures, and ii) the maximum level of deformation achieved. Concerning i), it is well acknowledged that martensite is a microstructural feature characterized by significantly lower corrosion resistance compared to austenite. Therefore, the higher the martensite content the lower the corrosion resistance. With regard to ii), it is worth noting that the samples were tested in terms of corrosion resistance at different strain values, namely e_{neck}, which were noticeably higher for the samples tested at sub-zero temperatures. It is recognized that the higher the level of strain hardening the lower the corrosion resistance due to the increased presence of dislocations.

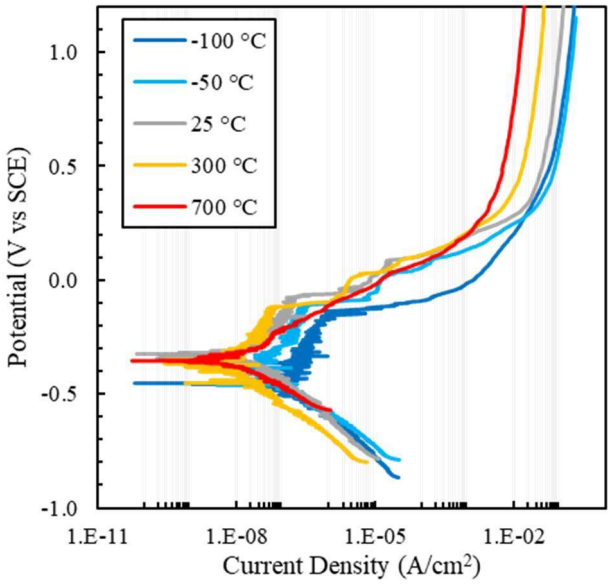

Figure 9. Potentiodynamic polarization curves recorded in 0.5 % saline solution as a function of the testing temperature for the *0 deg* samples.

Table 2. Corrosion data derived from Fig. 9.

T_{def} (°C)	e_{UTS} (−)	E_{corr} (V/SCE)	I_{corr} (μA/cm²)
-100	0.46	-0.45	0.2
-50	0.49	-0.39	0.7
25	0.41	-0.32	0.02
300	0.37	-0.38	0.009
700	0.15	-0.35	0.01

4. Concluding remarks

In this paper AISI 316 stainless steel samples were subjected to uniaxial tensile testing in a wide range of temperatures, from -100 °C to 700 °C. Their strain at UTS, namely the maximum strain for uniform elongation, was considered a measure of the steel ductility at varying temperatures and rolling directions. Afterward, the samples strained at UTS were analyzed in terms of microstructural features, micro-hardness and corrosion resistance.

The main following conclusions can be drawn:

- Deforming at sub-zero temperatures increases the UTS and uniform elongation, with a maximum average percentage increase of 16 % at -50 °C.
- Regardless of the considered section with respect to the rolling direction, the microstructure of the samples strained at UTS at sub-zero temperatures was always characterized by a certain amount of martensite, which increased as the deformation temperature decreased. On the contrary, no microstructural changes were evidenced when the deformation was carried out until UTS at 25 °C, 300 °C and 700 °C. The outcomes of the microstructural analysis were also confirmed by the XRD measurements.
- Regardless of the considered section with respect to the rolling direction, the hardness of the sample strained at UTS at -100 °C was the highest, as a consequence of the most significant SIMT effect, with a less significant influence in the case of the sample strained at UTS at -50 °C. The opposite situation was registered for the samples deformed within the warm forming range, whose hardness was reduced as expected.
- The corrosion resistance of the samples strained at UTS at sub-zero temperatures was substantially reduced compared to one of the samples deformed at room temperature and within the warm forming range. This corrosion reduction was ascribed to both the martensite presence and higher strain hardening.

Acknowledgements

This research was developed in the framework of the project "Sub-zero temperature forming processes for lightweight components - StepLight" ref. BIRD200305-2020 funded by the University of Padova, Department of Industrial Engineering.

References

[1] Takuda H, Mori K, Masachika T, Yamazaki E, Watanabe Y. Finite element analysis of the formability of an austenitic stainless steel sheet in warm deep drawing. J Mat Proc Tech 2003; 143-144: 242-248.

[2] Lu Q, Zheng J, Huang G, Li K, Ding H, Wang Z, Cheng S. Enhancing combined cryogenic mechanical properties of metastable austenitic stainless steel by warm forming. J Mat Proc Tech 2021; 291:117017

[3] Glazer J, Verzasconi SL, Sawtell RR, Morris JW. Mechanical behaviour of aluminium-lithium alloys at cryogenic temperatures. Metall Trans A 1987;18(10):1695-1701.

[4] Simonetto E, Bertolini R, Ghiotti A, Bruschi S. Mechanical and microstructural behaviour of AA7075 aluminium alloy for sub-zero temperature sheet stamping process. Int J Mechanical Sciences 2020;187:105919.

[5] Feng B, Gu B, Li S Cryogenic deformation temperature and failure mechanism of AA7075 alloy sheets tempered at different conditions. Mat Sci Eng A 2022; 848:143396.

[6] Liu W, Hao H. Damage and fracture prediction of 7075 high-strength aluminum alloy during cryogenic stamping process. Mechanics of Materials 2021;163:104080.

[7] Yuan S, Cheng W, Liu W, Xu Y. A novel deep drawing process for aluminum alloy sheets at cryogenic temperatures. J Mat Proc Tech 2020; 284:116743.

[8] Yang H, Li H, Sun H, Zhang YH, Liu X, Zhan M, Liu YL, Fu MW Anisotropic plasticity and fracture of alpha titanium sheets from cryogenic to war temperatures. Int J Plast 2022;156:103348.

[9] Zhang P, Wang H, Wang CJ, Zhu Q, Chen G. Effect of cryogenic temperature on the deformation mechanism of a thin sheet of pure copper at the mesoscale. Mat Sci Eng A 2021;822: 141714.

[10] Hussaini SM, Singh SK, Gupta AK. Formability and fracture studies of austenitic stainless steel 316 at different temperatures. J King Saud Univ-Eng Sci 2014;26(2):184-190.

[11] Aegerter J, Kühn HJ, Frenz H, Weißmüller C. EN ISO 6892-1: 2009 tensile testing: Initial experience from the practical implementation of the new standard. Materials Testing 2011;53.10:595-603.

[12] ASTM G5-14(2021) Standard Reference Test Method for Making Potentiodynamic Anodic Polarization Measurements.

[13] Tomita Y, Iwamoto T. Constitutive modeling of TRIP Steel and its application to the improvement of Mechanical Properties. Int J Mech Sci 1995; 37-12:1295 - 1305.

[14] Tsuchida N, Ueji R, Inoue T. Effect of temperature on stress–strain curve in SUS316L metastable austenitic stainless steel studied by in situ neutron diffraction experiments. ISIJ International 2021;61(2):632-40.

[15] Nohara K, Ono Y, Ohashi N. Composition and grain size dependencies of strain-induced martensitic transformation in metastable austenitic stainless steels. Tetsu-to-Hagané, 1977;63(5):772-782.